Recent developments in calorimetry for the linear e^+e^- collider

Leif Jönsson

Department of Physics,
Lund University, Lund, Sweden
E-mail: leif.jonsson@quark.lu.se

Abstract

The physics aims of the future electron-positron linear collider put strong demands on the performance of the detector. The calorimeter will play an essential role due to the importance of energy measurements, the reconstruction of jets and di-jet masses, missing energy measurements and lepton identification. Several new development projects are being worked on, with the aim of meeting the performance goals. A review of the present status is given.

1 Introduction

The main goals of a future e^+e^- linear collider in the energy range 500 GeV to 1 TeV is to offer a great exploration potential for new physics and at the same time allow for precision measurements of both standard model (SM) processes and in the region of physics beyond the standard model. Detailed studies of the top quark properties and precision measurements in the electroweak sector may already give hints about physics beyond the standard model. Even if the standard model Higgs has been discovered by the time the linear collider is realized, only the linear collider will enable detailed studies of its properties. The high energy of the collider is, however, mainly motivated by the possible direct discovery of new phenomena beyond the standard model like supersymmetry (SUSY). Many of the particles predicted by this theory can be investigated in quite some detail at the linear collider.

For a detector to meet these physics goals, high demands are put on the performance of the calorimeter. In order to illustrate the importance of the calorimeter and to specify its properties a few processes, including both standard model physics and physics in the SUSY sector, are being discussed briefly.

The dominant decay mode of t-quarks goes via a b-quark and a W-boson which results in a multi-jet final state with hard leptons and missing energy. The calorimeter thus needs to resolve the jets and provide good 2-jet mass resolution for the W-reconstruction. This requires high granularity over a large solid angle. Leptonic decays of W-bosons involve a significant amount of missing energy which needs a hermetic calorimeter with a coverage down to the smallest possible angels for precise measurements. Furthermore excellent lepton reconstruction is needed for the measurement of semileptonic decays.

The standard model Higgs boson is produced via either Higgs-strahlung ($e^+e^- \rightarrow ZH$) or WW-fusion ($e^+e^- \rightarrow \nu\nu H$). Except for the direct reconstruction of the Higgs mass from its decay, the Higgs-strahlung process also allows the Higgs mass to be determined via the recoil-mass technique for leptonic Z-decays. An accurate mass reconstruction of the Higgs boson, thus, requires good lepton and jet capabilities of a hermetic calorimeter with essentially 4π coverage. Another important decay mode of the Higgs boson goes into two photons, the measurement of which sets special requirements not only on the energy measurement of the photons but also on the directional information. Supersymmetric Higgs can be produced in the same kind of processes but also through pair production.

A characteristic signature of supersymmetric processes is the large missing energy in the event which is related to the fact that the lightest SUSY-particle, the neutralino, will leave the detector unobserved. Again a hermetic calorimeter is essential in order to achieve as good a determination of the missing energy as possible.

In supergravity models e^+e^- collisions may produce either a neutralino plus a gravitino or two neutralinos in the final state. If the lightest neutralino decays into a photon and a gravitino, which escapes detection, a pure photonic final state will be the result. Also the production and decay of heavier neutralinos could lead to just photons and missing energy in the detector. Since these photons are produced in the secondary vertices of decaying particles the typical signature of such processes is photons not pointing to the primary vertex. In order to obtain sensitivity to these decays it is necessary to provide the directional measurement of the photons with the calorimeter itself.

The conclusion of a conceptual study [1] was that the calorimeter must have the following properties:

- Hermeticity
- Longitudinal containment
- Good energy resolution
  $dE/E \leq 0.10/\sqrt{E} \oplus 0.01$ for the electromagnetic section
  $dE/E \leq 0.50/\sqrt{E} \oplus 0.04$ for the hadronic section
- High granularity
  0.9^ox0.9^o plus ≥ 3 longitudinal segments for the electromagnetic section
  2^ox2^o plus ≥ 3 longitudinal segments for the hadronic section
- Good reconstruction of photons and leptons

An important point to consider is whether any fraction of the calorimeter can be placed outside the magnetic coil and what consequences this will have on the measurements. The size of the coil, on the other hand, influences the strength of the magnetic field that can be obtained and this might have serious implications on the background situation in the region of the vertex detector. Thus, a good compromise must be found. Fig. 1 shows the energy deposition as a function of the calorimeter depth, given in interaction lengths (λ_{INT}), for pions at different energies. A clear peak after about one interaction length is observed followed by an exponential fall-off with λ_{INT}. The required depth of the electromagnetic calorimeter at the linear collider is about 1 λ_{INT} and thus inserting the

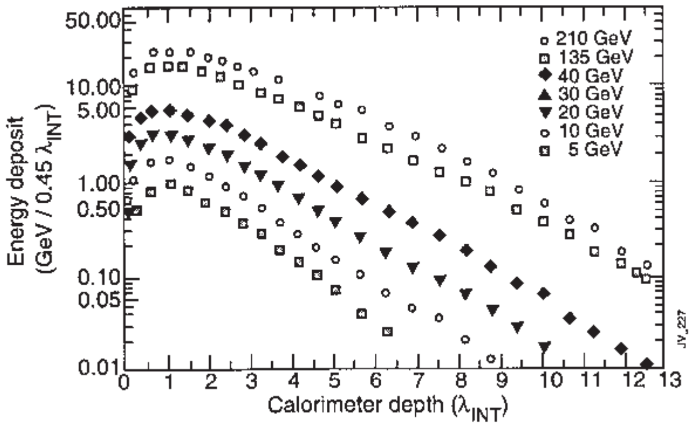

Figure 1: The energy deposition of pions at different energies as a function of the calorimeter depth.

coil after the electromagnetic section would deteriorate the energy resolution considerably, since it would introduce dead material corresponding to approximately 1.8 λ_{INT}. From the figure it is also clear that a total depth of at least 5 λ_{INT} is needed in order to absorb more than 95% of the energy at the highest energies. Decreasing the fraction of calorimeter inside the coil from 5 λ_{INT} to 2 λ_{INT} would according to simulations worsen the energy resolution by about a factor two. In addition the fraction of showers with more than 30 GeV missing energy increases from 3% to 7% [2]. The conclusion is that the full calorimeter should preferably be placed inside the coil which consequently requires a compact calorimeter so as to minimize the radius of the coil.

2 The Shashlik calorimeter

The idea behind the Shashlik calorimeter is illustrated in Fig. 2 and has been described in several previous papers [3] [4] [5] [6]. It consists of a stack of alternating absorber- and scintillating plates. Perpendicular to these plates a number of thin wavelengthshifting (WLS) fibres are running through holes in the plates. At the rear end of the stack the fibres are bundled together and connected to a photodetector. The blue light which is produced by the shower in the scintillating plates is picked up by the WLS fibres, shifted into green light and guided to the photodetector. The wavelength of the green light is well adopted to the sensitive region of various photodetectors available.

The test set-up which is under study for the future e^+e^--collider [7] provides a very fine sampling by using 140 layers of 1 mm lead absorbers and 1mm scintillating plates, corresponding to a total depth of about 25 X_o. The transverse dimensions of a tower were 5x5 cm^2 and the test set-up consisted of a square matrix with 25 towers. The towers were optically isolated from each other with white paper. The 1 mm diameter WLS fibres were distributed uniformly over the transverse area of the tower with a density of 1 fibre per cm^2. With this density the non-uniformity in the light yield can be kept as low as a few percent. In order not to loose light at the front end of the fibres, they were aluminized to make them reflective. Particles were prevented from traveling through the fibre holes, without interacting with the absorbing material, by mounting the calorimeter

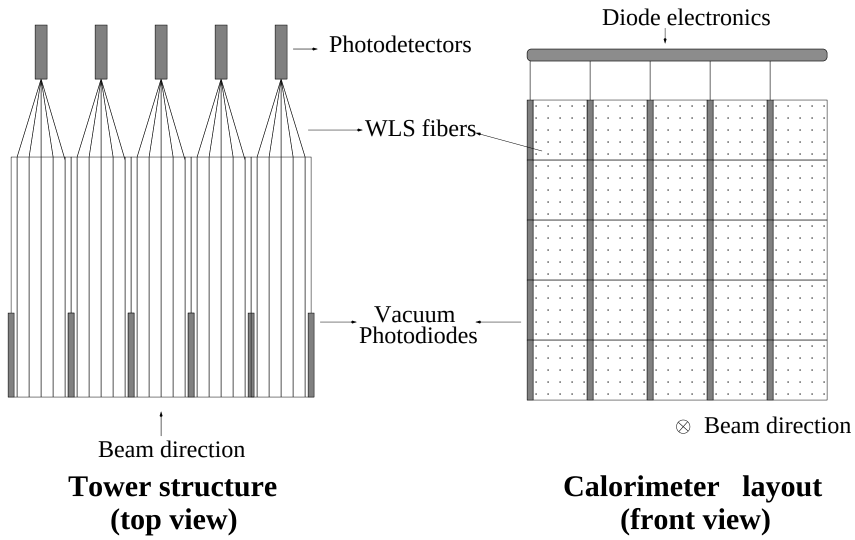

Figure 2: A Shashlik prototype calorimeter for the linear collider.

in a non-pointing geometry. Two types of fibres have been tested (Bicron BCF20 and Kuraray Y11) which both have light emissions at around 500 nm. The light was read out either by 1 inch phototetrodes from Hamamatsu or for some towers by avalanche photodiodes (APD), also from Hamamatsu, which have a very high quantum efficiency (80%). A plexiglass light guide was used to adapt the fibre bundle to the smaller sensitive area of the APD. Together with the photodetector also a preamplifier and a high voltage divider was mounted at the front-end of the set-up. The differential signals were then shaped and digitized.

In order to meet the requirement of longitudinal segmentation, which is needed to obtain separation between electrons and pions, vacuum photodiodes were mounted at the side of each tower covering a depth of $8X_o$ in the front part (see Fig. 2). The diodes stay in optical contact with the scintillating tiles and the light yield in the front part compared to the total light yield measured from the WLS fibres gives some information about the longitudinal development of the shower, which can be used for the e/π separation. This solution, however, introduces dead regions in the calorimeter, the consequences of which have to be evaluated carefully. Two different vacuum diodes are in use, both with a thickness of 5 mm but with sensitive areas of 28.9 cm^2 and 10.9 cm^2, respectively . The smaller area of the latter one allows for two diodes in a row and thus one additional longitudinal sampling. Unfortunately no results with the smaller vacuum diode exist from the first tests. The same read-out electronics as for the tetrodes was used, but positioned at the rear end of the towers.

Fig. 3 shows the energy resolution as a function of the electron beam energy. It is observed that the Kuraray fibre exhibit a much better performance than the Bicron fibre which is attributed to the fact that the latter one has a scintillating component. A parametrization of the curve for the Kuraray fibre gives:

$$\frac{\sigma(E)}{E} = \sqrt{\left(\frac{9.6\%}{\sqrt{E}} + 0.5\%\right)^2 + \left(\frac{0.130}{E}\right)^2} \tag{1}$$

which should be compared to a Monte Carlo simulation with Geant giving $6\%/\sqrt{E}$ for the first term. Since photoelectron statistics seems to be the dominant contribution

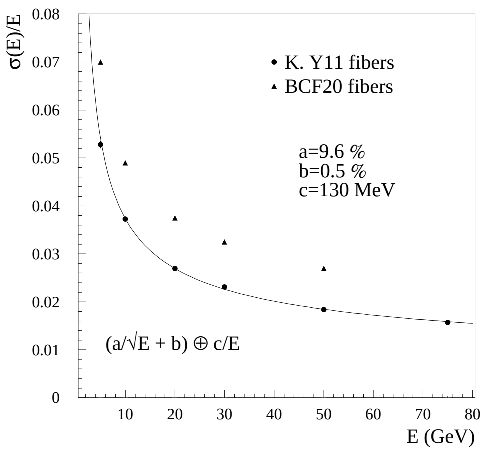

Figure 3: The energy resolution as a function of the test beam energy for two different WLS fibres.

to the measured resolution, the use of APD's should result in an improvement due to its high quantum efficiency. Unfortunately no tower was equipped with Kuraray fibres and APD read-out.

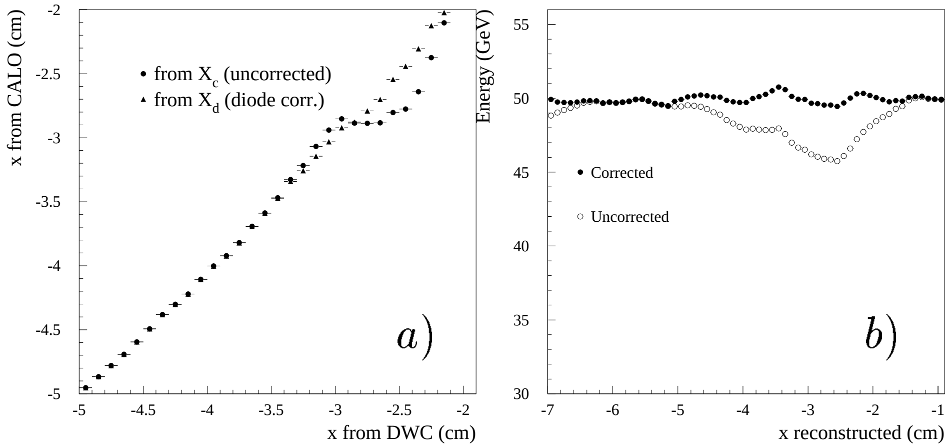

Figure 4: a) The spatial resolution and b) the energy response as a function of the test beam impact position.

The spatial resolution was investigated from scanning the electron test beam over the front face of the matrix. The impact position was calculated using the centre of gravity method [8]. Fig. 4 a) shows the reconstructed impact position compared to the beam position as measured by wire chambers in front of the calorimeter matrix (filled circles). There is a non-linear behaviour around -2.5 cm which is caused by the dead space due to the vacuum diode. The signal from the vacuum diode itself could, however, be used to correct for this non-linearity as seen in Fig. 4 a) (filled triangles). The position resolution was parametrized to have the following energy dependence:

$$\sigma_x(E) = \sqrt{\left(\frac{0.9}{\sqrt{E}}\right)^2 + (0.1)^2}\ cm \qquad (2)$$

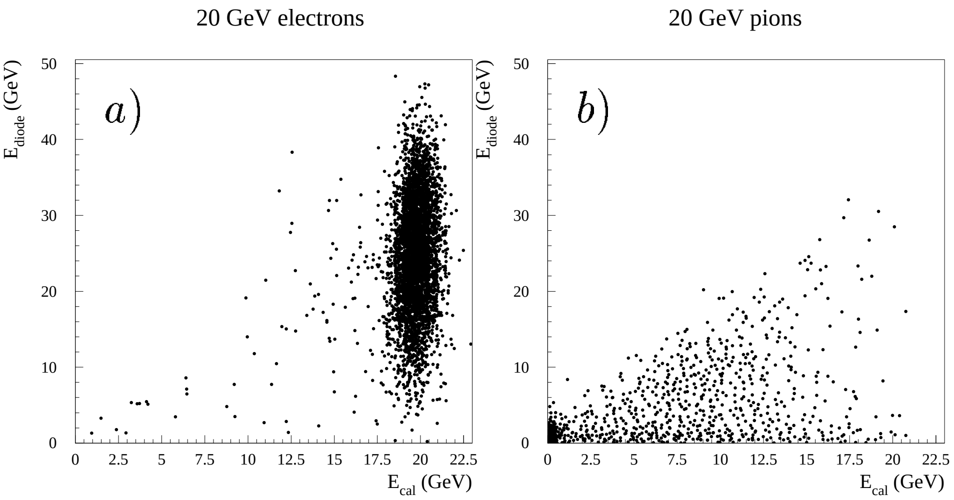

Figure 5: The energy deposition registered by the vacuum diode versus the total energy deposition for a) 20 GeV electrons and b) 20 GeV pions.

The energy response as a function of the beam impact position also exhibits a dip at the position of the vacuum diodes as seen in Fig. 4 b) (open circles). However, it is possible to parametrize the energy response as a function of the distance between the impact point and the vacuum diode and thus use the reconstructed impact point to apply a correction. The non-uniformity which remains in the corrected distribution (filled circles) is caused by the variations in light collection depending on the distance of the impact point to the WLS fibres.

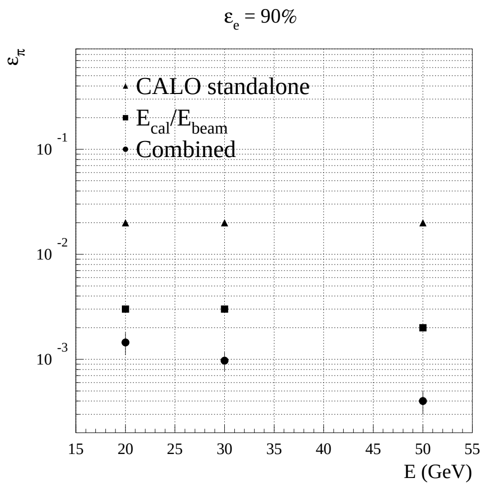

Figure 6: The pion contamination as a function of energy for 90% electron efficiency.

In order to discriminate between electrons and pions three different variables were used. The ratio of the energy measured by the calorimeter and the test beam energy, which in a real experiment has to be replaced by the particle momentum as measured in the tracking device; $\chi_E = E_{cal}/E_{beam}$. This ratio should be one for the electron and much smaller for the pion. Information on the longitudinal shower profile is obtained from the ratio between the energy read out by the vacuum diode and the total energy deposition of the shower; $\chi_D = E_{diode}/E_{cal}$. The response of a 20 GeV electron and a 20 GeV pion, respectively, is shown in Fig. 5 a) and b) where the energy deposition read out by the diode versus the total energy deposition is plotted. Also the lateral shower profile can be used for electron-pion separation. This is defined as $\chi_S = \sum_{i=1}^{N} E_i r_i^2 / \sum_{i=1}^{N} E_i$, where E_i is the energy deposit in the tower i, N is the number of towers contributing to the signal and r_i is the distance of tower i to the reconstructed impact point.

The results on the electron-pion separation are summarized in Fig. 6 where the pion contamination is plotted as a function of the energy, for 90% electron efficiency. It is seen that the application of the variable χ_E gives a factor of five lower pion contamination than using the pure calorimetric variable χ_D (CALO standalone). Combining both variables leads to further improvement.

Although it has been shown that the effects of the dead regions which are introduced by vacuum diodes placed at the sides of the towers can be compensated for in test beam situation, it is not evident that this is straight forward for complicated multi jet final states. It is also obvious that the Shashlik solution is not ideal for a finer lateral and longitudinal segmentation.

3 The Tile calorimeter

The segmentation problem of the Shashlik calorimeter could be overcome to some extent if the scintillating plates could be read out individually. Instead of bringing out the light via WLS fibres in the longitudinal direction of a toweras in the Shashlik case, a WLS-fibre can be positioned in a circular groove in each scintillator [2]. This fibre is connected to a waveguide fibre which brings out the light in a gap between the scintillator and the absorber to the read-out equipment outside the calorimeter, consisting of light mixing units, photodetectors, and multiplexing of the signals. Although the longitudinal segmentation in principle can be made very fine, the lateral segmentation will be limited by how small a bending radius that can be tolerated for the WLS-fibre in order not to suffer from losses in light. A rule of thumb is that the bending radius must be at least ten times the diameter of the fibre, which defines the lateral pad size to about 3 cm. In practice the pad size is limited by the number of waveguide fibres that can be accomodated in the gap where they are brought out and the number of read-out channels that can be afforded. Even if the pad size has to be increased, it is possible to improve the spatial resolution by taking advantage of the fact that a well defined tower structure is not needed for such a calorimeter. Thus, the pad layers can be shifted sideways with respect to each other and the pad size can be varied from layer to layer, which not only improves the spatial resolution but also enables projectivity without introducing cracks in the system. Further improvement of the spatial resolution might be obtained by using scintillator strip layers directed perpendicular to each other. Investigations of the scintillator pad calorimeter has just started.

A calorimeter with alternating absorber plates and silicon pad plates has been proposed in order to maximize the spatial resolution and to allow for a very fine longitudinal segmentation [9]. The ionization produced by the shower is measured in each pad plane and precise information on the shower profile, both laterally and longitudinally, will be obtained. The pad size is adjusted to the Molière radius of the absorber material. This solution offers excellent pointing properties which is especially important for final states with isolated photons where the vertex information can not be used.

One possible problem with this kind of calorimeter is the gap between the layers,

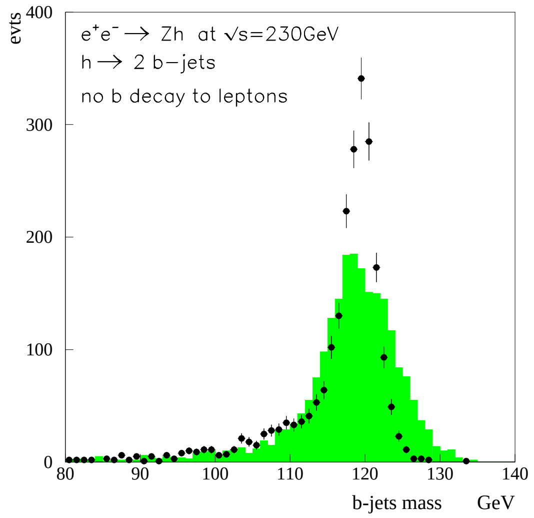

Figure 7: The di-jet mass resolution for $e^+e^- \rightarrow Zh$, where $h \rightarrow b\bar{b}$ at $\sqrt{s}$=230 GeV.

which is needed in order to bring out the signals. Very low momentum particles may, due to the magnetic field, move along the gap in a spiral trajectory and thus some of the shower energy may not be registered. Another disadvantage is the so far high cost of the Si-boards and the read-out electronics for the about $15 \cdot 10^6$ cannels which are foreseen for a fully equipped detector.

Simulations on the electromagnetic calorimeter performance have been performed using the Geant-4 program, assuming a 50 layer structure of 1.8 mm tungsten plus 300 μm silicon with a 2.7 mm air gap in between for the read out lines. For the hadron calorimeter a similar structure with 20 layers but with 2 cm iron plates as absorbers was used.

Since a large fraction of the jet energy is taken by charged particles the jet energy resolution from the calorimeter information alone will strongly depend on the magnetic field. With rising magnetic field a larger fraction of the energy will be carried by charged particles which do not reach the calorimeter at all or hit the calorimeter far from the shower centre of gravity. Using in addition the information from the tracking system considerably improves the energy resolution as illustrated in Fig. 7. The results have been obtained from simulations of a Higgsstrahlung process, $e^+e^- \rightarrow Zh$ at $\sqrt{s}$ = 230 GeV, where h decays into two b-jets at $\sqrt{s} = 230$ GeV. The histogram shows the di-jet mass resolution assuming $\Delta E/E_{e.m.} = 10\%/\sqrt{E} + 0.006$ and $\Delta E/E_{had.} = 40\%/\sqrt{E} + 0.01$. The resolution given by the points has been obtained with a much poorer calorimeter, $\Delta E/E_{e.m.} = 15\%/\sqrt{E}+0.01$ and $\Delta E/E_{had.} = 50\%/\sqrt{E} + 0.02$, but with the tracking information included. In spite of the poorer calorimeter the final mass resolution is significantly improved by using the measured particle momenta, making evident the importance of the tracker system.

The di-jet mass resolution is influenced by the ratio of photons overlapping with charged hadron tracks. Decreasing the fake rate from 15% to 10% will improve the mass resolution by almost 15%. An efficient separation of photon and hadron showers would thus provide a gain in mass resolution. The process $e^+e^- \rightarrow Zh$ where $h \rightarrow b\bar{b}$, was used again to illustrate the importance of having a high sensitivity to photons down to the lowest possible energy, and to be able to distinguish between showers induced by photons and charged particles at the smallest possible separation. With the use of a specific clustering algorithm for the tile calorimeter, a photon efficiency of 90% at 100 MeV was obtained,

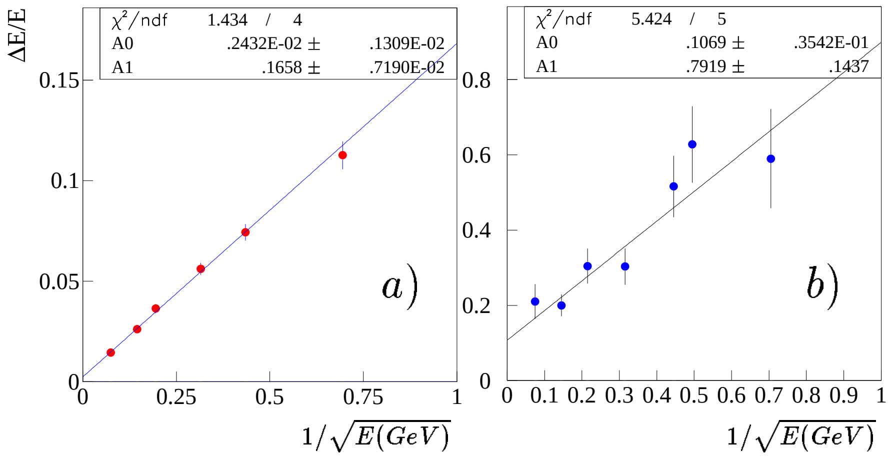

Figure 8: The energy resolution as a function of $1/\sqrt{E}$ for a) the electromagnetic and b) the hadronic calorimeters.

which increased to 100% above 300 MeV. It has also been proven, by simulations, that hadron and photon induced showers can be separated for impact positions as close as 1-2 cm, thanks to the excellent granularity.

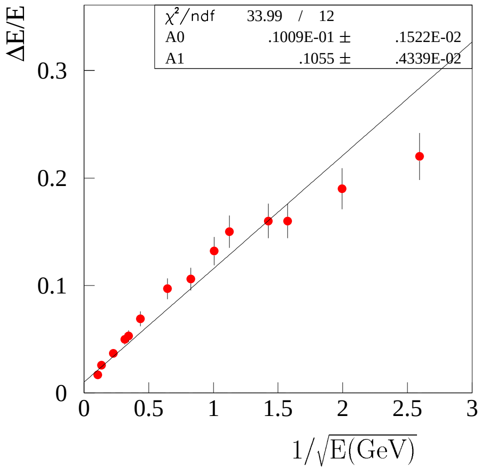

Figure 9: The energy resolution as a function of $1/\sqrt{E}$ for the electromagnetic calorimeter as the information on the particle multiplicity has been included.

The energy resolution of the electromagnetic and hadronic calorimeters are shown in Figs. 8 a) and b) as a function of $1/\sqrt{E}$. The resolution at 1 GeV is about 16% for the electromagnetic shower and 80% for the hadronic, which is far from the desired performance. Recently it has been demonstrated (Fig. 9) that the information on the particle multiplicity in the shower can be used to improve the electromagnetic energy resolution at low energies. However, this procedure has to be exploited further before definite conclusions can be drawn. The poor hadronic resolution is due to fluctuations of the π^o content in the hadronic shower and the unequal calorimeter response for electromagnetic and hadronic energy. This, however, can be compensated for by using a software energy weighting technique, which relies on the fact that local energy deposits of high density are mainly of electromagnetic origin. Thus, if the calorimeter is well segmented a statistical

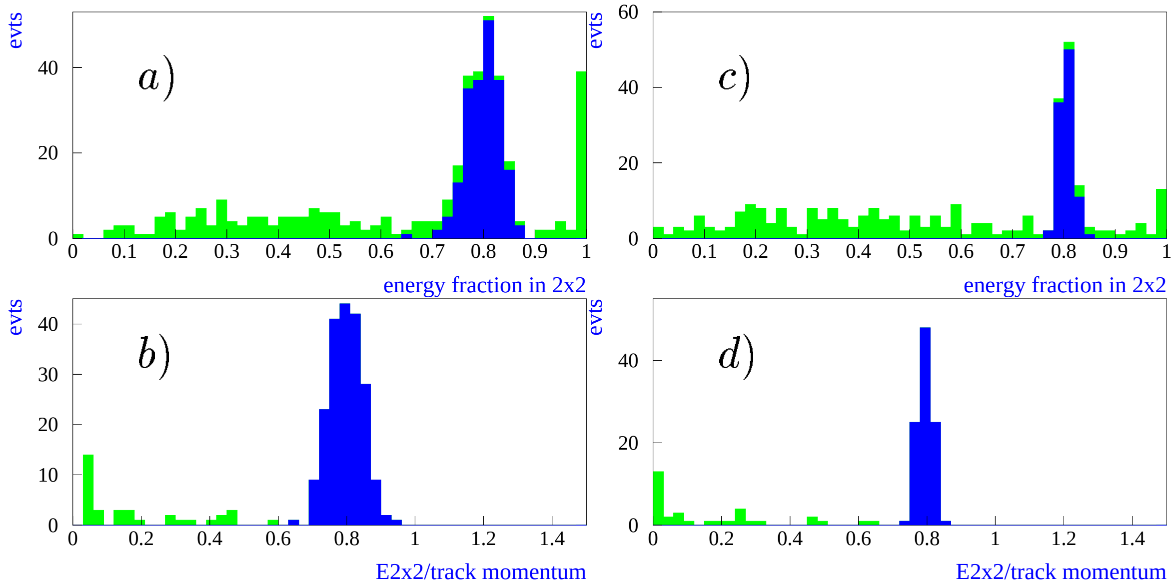

Figure 10: The e/π separation at 10 GeV and 50 GeV using the calorimeter alone compared to including the information from the tracking system.

separation of the electromagnetic and hadronic energy depositions can be achieved. With this technique the hadronic energy resolution can be improved to around 40%.

Fig. 10 compares the energy spectra of electrons (black histogram) and pions (shaded histogram) at 10 GeV (Figs. 10 a) and b)) and 50 GeV (Figs. 10 c) and d)) as measured by the calorimeter alone (Figs. 10 a) and c)) and taking advantage of the information on particle momenta from the tracker (Figs. 10 b) and d)). The separation between electrons and pions improves considerably as the tracking information is used. Quantitatively, the result is that the pion contamination is less than $6 \cdot 10^{-3}$ at 90% C.L. for 100% detection efficiency of the electrons.

In order to avoid the cost problem with the Si-pad read-out, a combination of Si-pads in the first calorimeter sections and scintillating pads for the rear part might offer an interesting option which combines good performance with reasonable cost.

4 The Crystal calorimeter

Crystal calorimeters are known to give the best possible energy resolution for electromagnetically interacting particles due to the ideal uniform mixture of the absorbing material and the active component. They are not so well suited for hadrons since the response to electromagnetic and hadronic energy is considerably different and a longitudinal segmentation of the crystals, which is necessary for compensation by energy weighting, causes a problem. Several large scale calorimeters have been built over the last couple of decades using different types of crystals, governed by the experimental conditions [10] [11] [12] [13] [14] [15] [16] [17] [18].

As an illustration of the good electromagnetic energy resolution of crystal calorimeters, measurements with the BGO calorimeter of the L3 experiment at LEP [12] are shown in Fig. 11 a), and in Fig. 11 b) the expected energy resolution of the $PbWO_4$ calorimeter, built for the CMS experiment at LHC, is given. In the latter case the various contributions

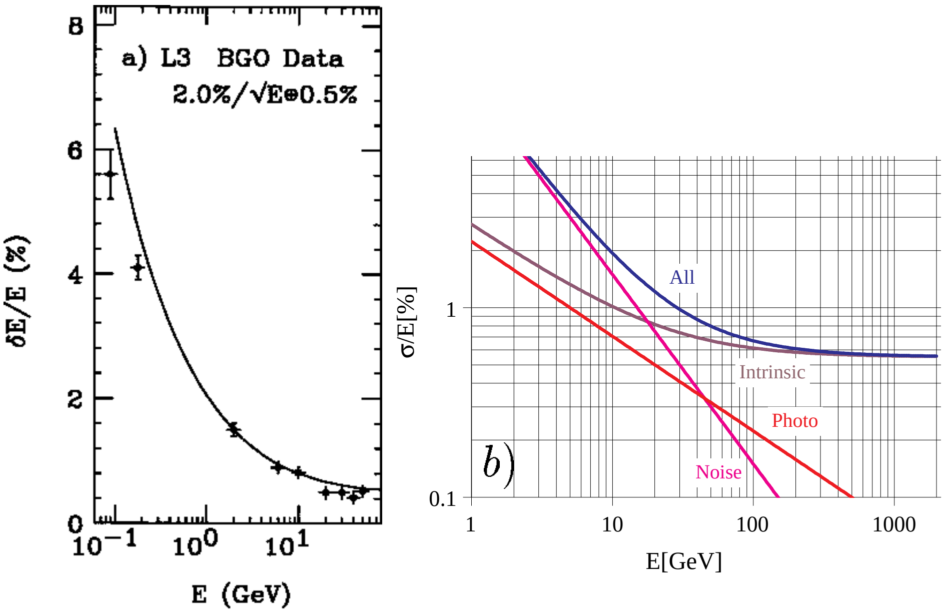

Figure 11: The energy resolution of a) the BGO calorimeter in the L3 experiment as measured in a test beam, and b) the designed energy resolution of the $PbWO_4$ calorimeter for the CMS experiment.

from photoelectron statistics, electronic noise and intrinsic effects (systematics) are shown separately. Beyond 20 GeV the energy resolution is limited by systematic terms due to geometry effects, intercalibration errors and non-uniformities in the crystal response. For the BGO measurements the data points are compared to a parametrization of the form $2\%/\sqrt{E} \oplus 0.5\%$. For energies higher than 20 GeV the crystal calorimeters reach sub-percentage precision.

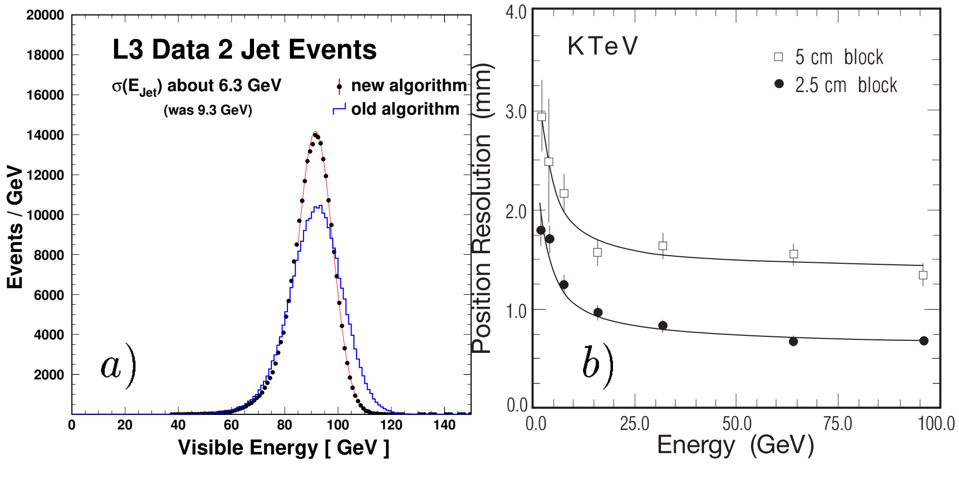

Figure 12: a) The di-jet mass resolution for Z^o decays measured by the L3 collaboration and b) the spatial resolution as a function of the test beam energy obtained by the KTeV collaboration.

The di-jet mass resolution from decays of Z^o-bosons, as measured by the L3 detector, is shown in Fig. 12 a). Using the calorimeter alone (old algorithm), the width of the Z^o

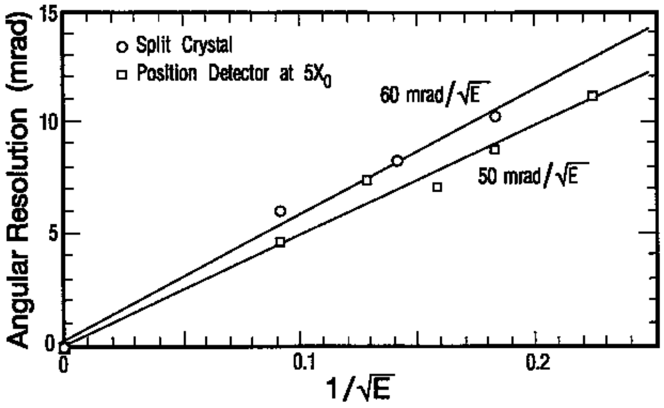

Figure 13: The angular resolution as a function of $1/\sqrt{E}$ measured for a CeF_3 calorimeter by the CMS collaboration.

peak is measured to 9.3 GeV, corresponding to a mass resolution of 10%, whereas the inclusion of the tracker information (new algorithm) decreases the width to 6.3 GeV (7% resolution).

The spatial resolution, which has been obtained from centre of gravity reconstruction on the CsI calorimeter of the KTeV collaboration, is shown in Fig. 12 b) [15]. A lateral cell size of 5 cm and 2.5 cm results in resolutions down to 1.4 mm and 0.8 mm, respectively.

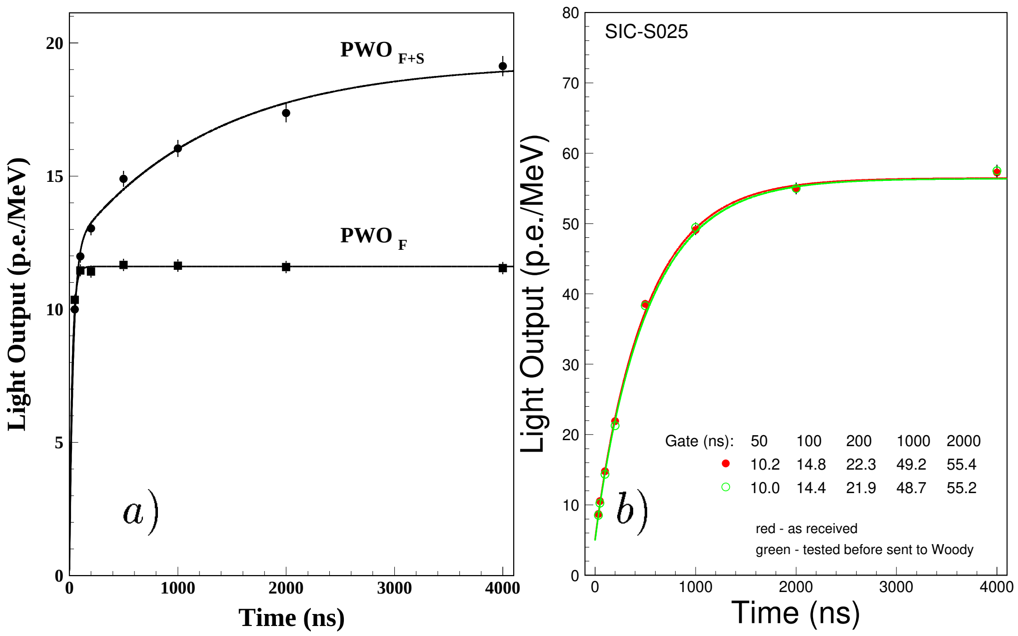

Figure 14: The light yield of two different $PbWO_4$ crystals as a function of the light collection time.

In order to measure the direction of photons by a crystal calorimeter, it has to be segmented in depth. Two approaches have been studied. One is to just segment the crystal into two pieces and the other is to use a fine grained position detector in between the longitudinal segments. Fig. 13 presents the results from a GEANT simulation on a CeF_3 calorimeter with, on one hand, a longitudinal segmentation into two pieces of 8 X_o

and 17 X_o, which are read out separately, and, on the other hand, introducing a position detector after 5 X_o. An angular resolution of as good as 50 mrad/$\sqrt{E}$ was obtained. More sophisticated methods of splitting the crystals have also been considered in order to further improve the angular resolution. It should however be realized that this method only works for high energy photons which produce showers of sufficient length to provide signals without great fluctuations in both segments.

In Fig. 14 a) the light yield as a function of the integration time is shown for $PbWO_4$ crystals. The lower curve represents the light yield from the fast component, which amounts to 12 photoelectrons/MeV and doesn't depend on the integration time. A significant gain is, however, obtained from the slow component if the integration time can be increased up to the order of microseconds. Recently a much brighter $PbWO_4$ crystal has been produced, giving 56 photoelectrons/MeV for an integration time of 2 μs (Fig. 14 b). The emission spectrum of this crystal is peaked at 520 nm which fits well to the quantum efficiency of existing photo cathodes.

Relevant crystal properties which have to be considered in order to adjust to the experimental situation are density, radiation length, Molière radius, light yield, wavelength of light, decay time, temperature dependence and radiation hardness. A comparison of some materials are given in Table 1.

Table 1: Some important properties of a selection of crystals

Crystal	NaI(Tl)	CsI(Tl)	CsI	PbF_2	BGO	$PbWO_4$
Density (g/cm^3)	3.67	4.53	4.53	8.24	7.13	8.28
Radiation Length (cm)	2.59	1.85	1.85	0.9	1.12	0.9
Molière radius (cm)	4.5	3.8	3.8	2.2	2.4	2.2
Hygroscopicity	yes	slight	slight	no	no	no
Luminescence (nm)	410	565	420		480	520
(at peak)			310			420
Decay time (ns)	250	1000	35		300	50
			6			10
Light yield (relative)	100	45	5.6		15	0.3
			2.3			1.0

The calorimeter for the linear collider detector has to be compact since it has to fit inside the magnetic coil. This immediately excludes some of the materials like NaI and CsI. An additional complication with NaI is that it is hygroscopic and therefore a special container with dry air is required. BGO is a dense material but the decay time is relatively slow and its price per cc is high due to the expensive raw material. PbF_2 has been used as Cerenkov material, but attempts have been made to dope it with different materials to make it scintillating. The results are so far inconclusive.

5 Calibration

In order to profit from the potentially good energy resolution of the calorimeter it is of utmost importance to perform precise calibration in a test beam before installation and *in situ* during the runs. The purpose of the test beam calibration is to define the absolute energy scale of the calorimeter and to understand its behaviour. This can only be performed for a limited number of modules. Measurements *in situ* should also provide the channel-to-channel variations with time. Several different methods have been used for the *in situ* calibration.

One possibility is to take advantage of well-known physics processes with final state particles of known energy, pair production from decays of particles with precisely known mass, low energy particles with their momenta accurately measured in the tracking system or minimum ionizing particles, like muons from cosmic rays or beam halo muons. At the linear collider the production of e^+e^- pairs from Bhabha scattering or the reconstruction of Z^o decays are examples of processes which can be used. Dedicated runs at the Z^o peak will be necessary to collect enough statistics.

Radioactive sources can also be used for calibration purposes. The advantage is that they are small and can be mounted directly on the calorimeter cells where they will provide continuous calibration information. The disadvantage with this method is the limited energy range which can be covered. More complicated arrangements with beams from external accelerators have been used in the Crystal Ball and the L3 experiments.

A frequently used method for intercalibration is based on light pulsers. A light source which is placed outside the detector illuminates a bundle of optical fibres, from which the fibres are distributed to the individual cells. A reference system is used to monitor the intensity of the light to get the right normalization. The method relies on the assumption that it is possible to achieve a uniform distribution of the light over the fibre bundle so that each fibre carries the same amount of light. It is also important that the optical properties of the fibres are not influenced by radiation. The system is reliable and easy to operate.

The experience has shown that it is important to combine several different methods to cover a wide energy range and to get sufficient understanding of systematic effects.

6 Summary

For the ambitious physics programme at the future e^+e^- linear collider the calorimeter is one of the most important components of the detector. The main purpose of the calorimeter is to deliver information on the energy carried by charged and neutral particles. Many final states include multiple jets, which have to be measured accurately and furthermore a good di-jet resolution is needed for mass reconstruction. Hence, the calorimeter should provide excellent energy resolution and angular information, which implies fine longitudinal and lateral segmentation. The calorimeter is also essential for measuring missing energy, which is the characteristic signature of SUSY particles and neutrinos. For this a hermetic calorimeter which cover as much as possible of the solid angle should be aimed at. Good lepton identification is important in order to recognize semileptonic decays.

The recent development in calorimetry, to meet the requirements set by the physics programme at the linear collider, follows a few different lines, like the Shashlik, tile and crystal technologies. Calorimeters with exotic liquids as active material has also been looked into, but these require special containers which will deteriorate the hermeticity and the energy resolution.

There is much work to be done until it is clear which technique is superior and can still be affordable.

7 Acknowledgement

I am greatful to P. Checchia, J.-C. Brient, V. Korbel, and R.Y. Zhu for providing me with the necessary information. R. Heuer, V. Korbel and U. Mjörnmark are acknowledged for comments and remarks to the content of this article.

References

[1] Conceptual Design of a 500 GeV e^+e^- Linear Collider with Integrated X-ray Laser Facility, eds. R. Brinkmann et al., DESY 1997-048, ECFA 1997-182 (1997)

[2] V. Korbel, private communication

[3] J. Badier et al., Nucl. Instr. and Meth. **A348** (1994) 74

[4] HERA-B design report, DESY/PRC 95-01

[5] LHCb technical proposal, CERN/LHCC 98-4

[6] S.J. Alsvaag et al., CERN/EP 98-132

[7] A.C. Benvenuti et al., Phys. Lett. **B376** (1996) 193

[8] G.A. Akopdjanov et al., Nucl. Instr. and Meth. **140** (1977) 441

[9] J.-C. Brient, private communication

[10] M. Oreglia et al., Phys. Rev. **D25** (1982) 2295

[11] T. Böringer et al., Phys. Rev. Lett. **44** (1980) 1111; G. Mageras et al., Phys. Rev. Lett. **46** (1981) 1115

[12] L3 Collaboration, Nucl. Instr. and Meth. **A289** (1990) 35

[13] Y. Kubota et al., Nucl. Instr. and Meth. **A320** (1992) 66

[14] E. Aker et al., Nucl. Instr. and Meth. **A321** (1992) 69

[15] K. Arisaka et al., KTEV design report, FN-580 (1992)

[16] Babar Collaboration., Technical design report, SLAC-R-95-457 (1995)

[17] BELLE Collaboration, Technical design report, KEK Report 95-1 (1995)

[18] Compact Muon Solenoid Technical Proposal., CERN/LHCC 94-38 (1994) (1996) 193